Experimental and Numerical Investigations on Propagating Modes of Detonations: Detonation Wave/Boundary Layer Interaction

Xiaodong Cai[1], Jianhan Liang[1]*, Ralf Deiterding[2]

Yasser Mahmoudi[3], Mingbo Sun[1]

[1]Science and Technology on Scramjet Laboratory

National University of Defense Technology, Changsha, 410073, China

[2]Aerodynamics and Flight Mechanics Research Group, University of Southampton

Highfield Campus, Southampton SO171BJ, United Kingdom

[3]School of Mechanical and Aerospace Engineering, Queen's University Belfast,

Belfast BT9 5AH, United Kingdom

*Corresponding author: jhleon@vip.sina.com

Abstract: In the present work the propagating modes of detonation wave in supersonic hydrogen-air mixtures are investigated in narrow rectangular channels. To clarify the effect of the detonation wave interaction with the boundary layer on the evolution and propagation of detonation phenomenon, high-speed laser schlieren experiments and adaptive Navier-Stokes (NS) simulations (pseudo-DNS) combined with a detailed reaction model are performed. The experimental results show that after successful ignition, two propagating modes are observed and can be classified as Oblique shock-induced combustion/Mach stem-induced detonation (OSIC/MSID) and pure Oblique shock-induced combustion (OSIC). For the OSIC/MSID mode, a

Mach stem induced overdriven detonation is generated in the middle of the main flow. For the pure OSIC mode, no detonation wave but two oblique shock-induced combustion regions are generated throughout the whole channel with the overall structure taking a thwartwise V shape. The OSIC/MSID and pure OSIC propagation modes are further confirmed by pseudo-DNS employing a detailed reaction model and dynamic adaptive mesh refinement for the same conditions as utilized in the experiments. The numerical results show that because of subsonic combustion near the walls induced by the boundary layers, the OSIC/ MSID is not entirely symmetrical, while for the pure OSIC mode, larger fluctuations are observed along the oblique shock waves resulting from enhanced instabilities due to additional chemical heat release.

***Keywords*:** Supersonic combustible mixture; Detonation wave/boundary layer interaction; Propagation modes; Hot jet initiation

1 Introduction

Thanks to the superior performance at high Mach numbers (normally Ma>5), the scramjet has become one of the first choices for hypersonic air-breathing propulsion systems [1]. Nowadays, the scramjet is getting close to the actual engineering application due to several decades of development. It is well known that due to the inherent theoretical advantage over deflagrative combustion, detonative combustion has been investigated extensively for propulsion applications [2-4]. It is believed that the performance of scramjets is expected to be improved significantly if a full or even a local detonation could be realized already in the incoming supersonic combustible flow, which can be newly named as detonation-driven scramjet (DDS). In addition, it is expected that the DDS can be suitable for higher flight Mach numbers than the

conventional scramjet. Based on this idea, we have conducted a series of numerical simulations [5-8] on detonation combustion in supersonic combustible mixtures using a hot jet initiation. The adaptive mesh refinement open-source program AMROC (Adaptive Mesh Refinement in Object-oriented C++) [9-11] based on the Structured Adaptive Mesh Refinement (SAMR) approach [12-13] had been adopted to solve the reactive Euler equations with simplified [14] and detailed reaction models [15] using a robust second-order accurate MUSCL-TVD scheme. Qualitatively correct conclusions can be obtained using the inviscid Euler equations. However, some nonphysical substructures may be generated in detonation simulations at high grid resolution. Oran et al. [16] conducted a series of detonation simulations using both the Euler and Navier-Stokes (NS) equations with a detailed reaction model, and observed similar detonation structures. They noticed that the small-scale structures, which are not present when using the Euler equations, do not have an obvious influence on the overall detonation features. It should be noted however that only regularly oscillating detonations were considered in these simulations [16]. Mazaheri et al. [17] suggested from a comparison between the Euler and Navier-Stokes (NS) solutions, that diffusion effects play no major role in regularly oscillating detonations as hydrodynamic instabilities such as Kelvin-Helmholtz (KH) and Richtmyer-Meshkov (RM) instibilities are generally absent. Conversely, in irregular detonations hydrodynamic instabilities can generate a turbulent mixing zone of the burned products and unburned reactants, and therefore diffusive turbulent mixing can play a key role in detonation structure development, indicating that the NS equations should be solved

in this case. Mahmoudi et al. [18] showed that hydrodynamic instabilities described by the Euler and NS equations alone are not sufficient to ensure full consumption of the unburned reactants behind the shock front. They pointed out that the effect of vorticity generation and energy dissipation at the subgrid scales (SGSs) plays an essential role in burning the unburned gases in this region. Paolucci et al. [19-20] employed the Wavelet Adaptive Multiresolution Representation (WAMR) method including detailed diffusive transport and chemical kinetics models for both one-dimensional and two-dimensional viscous hydrogen detonation simulations. They found that small inhomogeneties in species massfractions are observed due to multicomponent diffusion and indicated that a grid spacing of 15 microns is necessary for viscous calculations. Ziegler et al. [21] carried out direct numerical simulations of the multicomponent, compressible, reactive NS equations to investigate the accurate solution of diffusive processes within reaction zones. It was demonstrated that there is a clear difference between simulations with and without diffusive transport in the region of the shear layers and jetting, and it was shown that diffusion dramatically affects the presence of the large-scale structures in the shear layer, features that are very prominent [14] in inviscid detonations. Compared with the Euler equations, solving the NS equations in detonation simulations is theoretically more reliable for actual applications, and has become a topic of recent research interest. Using the two-dimensional reactive NS equations with one-step Arrhenius kinetics, Gamezo et al. [22-23] computed the flame acceleration and DDT in channels with obstacles. They reproduced the main regimes of flame propagation observed in experiments, and

studied flame acceleration and DDT phenomena for different obstacle spacings. In order to investigate the mechanism of flame acceleration and DDT in large obstructed channels, Kessler et al. [24] carried out extensive two- and three-dimensional simulations of detonation structures using the reactive NS equations and one-step chemistry models with diffusive transport of a stoichiometric mixture. It was found that using the simple reaction model qualitatively and quantitatively matches the experiments, which are largely insensitive to small variations in model parameters. Goodwin et al. [25-26] studied DDT and the effect of decreasing blockage ratio in small channels with obstacles by solving the multidimensional reactive NS equations with one-step Arrhenius kinetics, mainly presenting two types of simulations: one with DDT occurring in a gradient of reactivity and another in which DDT arises from energy focusing as shocks converge. Cai et al. [27] investigated the diffusion and mixing effects in hot jet initiation and propagation of hydrogen detonations using the two-dimensional reactive NS equations with one-step Arrhenius kinetics. They pointed out that compared with the inviscid case, the diffusion effect in the viscous detonation can play a more significant role in the suppression of the oscillating instability at the detonation front, thus eventually altering the triple point generation mechanism, even with a larger overdrive degree.

From the above literature review it is imminent that viscosity cannot be neglected when modelling detonation initiation and development. Yet, aside of small-scale structures in the detonation front, viscosity has generally a negligible influence on detonation propagation in free space and classical theory thereby

assumes a strictly inviscid model. This picture however changes entirely for continuous quasi-steady detonations in narrow channels, as they would invariably occur in any DDS device. The combustion chamber of a DDS is basically a duct with supersonic inflow, which generates turbulent boundary layers on the channel walls. It is well known from experiments and computations that interactions of shocks and boundary layers result in shock bifurcations and the appearance of oblique shocks and vortices [28]. Rather few studies of shock and boundary layer interactions have been conducted in combustible mixtures though. Gamezo et al. [29] conducted reactive NS simulations to examine the effects of bifurcated shock structures on shock-flame interactions and DDT in shock-tube experiments. They studied an important process for the interaction of the reflected shock with the boundary layer formed by the incident shock, and found that the interaction leads to bifurcation of the reflected shock and the formation of a complex structure containing a leading oblique shock followed by a recirculation region, indicating that the boundary layer interaction can have a noticeable effect on how, when, and where DDT occurs. Flame acceleration and DDT were simulated using the reactive NS equations with the single-step reaction model by Oran and Gamezo [30]. They reported that the boundary layers through the interactions with shocks and flames can help to create environments in which hot spots can develop. Grogan and Ihme [31] performed detailed simulations of hydrogen-oxygen mixtures employing a second-order accurate NS equations solver to study weak and strong ignition regimes in a shock-tube system, and found that the thermal boundary condition at the solid wall has a significant impact on the ignition

mode in shock-tube simulations: the adiabatic boundary condition can heat the boundary-layer fluid by viscous-dissipative effects, while the isothermal boundary condition is physically more justifiable. Further, they investigated the regimes of shock boundary layer interaction in consideration of shock tube kinetic experiments and examined three ways that the reflected shock wave interacts with the boundary layer: incipient separation, shear layer instabilities and shock bifurcation [32].

The investigations decribed above have provided significant insights into the phenomenon of detonation or shock wave interaction with a boundary layer. We recently computed two-dimensional high-resolution detonation simulations in a supersonic hydrogen-oxygen mixture using the reactive NS equations in expanding channels [33]. In order to eliminate the complexity of detonation interaction with the boundary layer and to be able to focus the study just on the detonation propagation in the expansion section, in Ref. [33] we had employed the slip-wall boundary condition for an otherwise viscous model in order to avoid dealing with boundary layers produced in the inflow section. Although qualitatively correct results were still obtained [34], considering the actual supersonic flight condition, it is necessary to consider the effect of detonation/shock interaction with the boundary layer in order to obtain an accurate description of the detonation evolution and its propagation. Following the previous study, the objective of this paper is to examine the detonation evolution and its propagating mode in supersonic combustible mixtures considering the detonation/shock wave interaction with the boundary layer using the experimental

observations together with adaptive NS simulations with a detailed reaction model [15].

The remainder of the paper is organized as follows: the experimental system and calculations method are introduced in Section 2. The experimental results are shown in Section 3, in which the hot jet initiation and especially propagating modes of detonation in supersonic combustible mixtures are studied. The corresponding numerical results are presented in Section 4, in which the propagating mode in the supersonic combustible mixture is discussed compared with the experimental observations. Finally, Section 6 concludes the paper.

2 Experimental system and calculation model

2.1 Experimental system

2.1.1 Experimental setup

The experiments are carried out in a supersonic test rig, as depicted in Fig.1(a). A high-temperature oxidizable flow is first generated from the combustion of the H_2/O_2/Air mixture in an air preheater. It is required that the mass fraction of the oxygen in the produced oxidizable flow equals 23%. Therefore, through the control of the molar ratio of the H_2/O_2/Air mixture, it is able to replicate an actual air mixture. This oxidizer flow is then accelerated to supersonic flow in a Laval nozzle with the design Mach number 3.0. The premixing duct downstream of the nozzle is designed for premixing of the oxidizer flow with the additional hydrogen injected independently within the Laval nozzle upstream of the test section, which has been demonstrated for a high degree of premixing [35]. Finally, a supersonic combustible

flow with specified Mach number, pressure, temperature and molar ratio is created. Glass windows are installed on the side walls of the test section for optical access. The whole test rig is connected with a vacuum tank for the gas dumping.

In previous works [35-36], a single window was used for optical observation. However, due to the limitation of the window length, only the hot jet initiation process could be effectively observed. Yet, when detonation initiation is realized in the supersonic combustible mixture, it is likely to propagate forward towards the incoming flow. Therefore, when only a single window was installed, it became rather difficult to directly observe the propagating detonation in its entirety. Compared with the single window, the double-window setup can increase the observation length, thus providing more chances for observing the propagating detonation. As shown in Fig.1(b), the double windows (the first window Win 1 and the second window Win 2) with the distance of 43 mm have the same extensions of height 42 mm, width 32 mm and length 80 mm. Ignition is provoked by a hot jet. As shown in Fig.1(b), a hot jet tube with an exit diameter of 4 mm is installed on the top wall of Win 1 with a distance of 25 mm from the left side of Win 1 as an igniter. The tube is filled with a stoichiometric hydrogen/oxygen mixture whose chemical reactivity can be adjusted by changing the mixture pressure. The combustible mixture in the tube, provided with an independent supply system, is first ignited using a spark plug to produce a hot jet with high temperature and pressure, and then through a sonic exit the hot jet is perpendicularly injected with a sonic speed at the downstream end of the test section after steady state is reached. The hot jet initiates reaction, which leads to very fast

pressure rise and propagation of the flame although the approach flow is supersonic.

2.1.2 Optical observation and pressure measurement

Three pressure sensors (P1, P2, P3) are set up on the top wall of Win 2 for pressure measurement. The maximal response frequency of the sensors is 30 kHz with a measurement resolution of 0.05% FS. The pressure sensors are distributed equally with a distance of 20 mm, and are also 20 mm away from both sides of the window. A high-speed laser schlieren apparatus is utilized for continuous optical observation. The maximal shooting speed of the camera is 10^6 fps with a shortest shutter time of $1/2.73\times10^6$ s. The temporal resolution is less than one microsecond and thereby capable of producing frozen snapshots of the detonation combustion. The laser is used for continuous illumination, which eliminates disturbances of the detonation flame and allows decreasing the camera shutter time to the minimum.

2.2 Calculation model

2.2.1 Computational setup

In order to compare with the experimental results, the detonation simulations described here are conducted for the same condition as the experiment. For computational efficiency, the ignition phase including hot jet injection and DDT are not considered and a fully developed inviscid ZND profile is used throughout the domain width instead. The size of the observation window in Fig.1(b) is fitted with the computation domain with a length of 80 mm and a height of 42 mm. Adiabatic no-slip boundary conditions are used on the upper and lower walls. The right boundary is given a supersonic inflow condition and the left one is set to an ideal

outflow boundary condition. Although a hot jet is adopted for detonation initiation in the experiments, in order to eliminate the complexity of the hot jet initiation and to be able to focus the present study just on the propagating mode in the supersonic combustible mixtures, we have opted to use the Zel'dovich-von Neumann-Döring (ZND) solution as the initial flow field. The detonation front in the ZND solution is placed at a sufficient distance from the right inflow boundary to ensure the boundary layer development, hence being able to directly investigate detonation wave interaction with the boundary layer. The detonation front in the ZND model is placed at a distance of 50 mm away from the left outflow boundary. The $H_2/O_2/N_2$ mixtures under pressure 36.1 kPa and temperature 581 K with the molar ratio 0.56:1.0:2.9 and 0.58:1.0:2.9, respectively, are adopted as the supersonic incoming flows entering from right to left at a velocity of 1532 m/s. Calculated by Cantera, the induction length of the one-dimensional ZND model under the above condition is approximately $l_{ig} = 2.15$ mm. It should be noted that this initialization approach would affect the overdrive degree of the detonation slightly compared to hot jet ignition [34, 37]. However, in three-dimensional channels, the hot jet injection only occupies a very small part of the whole flow field, thus not being able to set up the contractive passway effectively for overdriven propagation [38]. Therefore, it is not expected that this setup will play an influential role in the observed propagation mode.

2.2.2 Governing equations

The reactive compressible flow field is governed by the reactive Navier-Stokes (NS) equations in combination with a detailed chemistry model. The two-dimensional

governing equations are expressed as follows:

$$\frac{\partial U}{\partial t}+\frac{\partial (F_{conv}-F_{diff})}{\partial x}+\frac{\partial (H_{conv}-H_{diff})}{\partial y}=S_{chem}, \tag{1}$$

$$\boldsymbol{U}=(\rho,\rho u,\rho v,\rho e_t,\rho_1,\cdots,\rho_{K-1})^T, \tag{2}$$

$$S_{chem}=(0,0,0,0,\dot{w}_1,\cdots,\dot{w}_{K-1})^T, \tag{3}$$

$$\begin{aligned} F_{conv}&=\begin{pmatrix}\rho u\\ \rho u^2+p\\ \rho uv\\ (\rho e_t+p)u\\ \rho_1 Y_1 u\\ \vdots\\ \rho_{K-1}Y_{K-1}u\end{pmatrix} \quad F_{diff}=\begin{pmatrix}0\\ \tau_{xx}\\ \tau_{xy}\\ u\tau_{xx}+v\tau_{xy}-q_x\\ \rho_1 Y_1 V_{x,1}\\ \vdots\\ \rho_{K-1}Y_{K-1}V_{x,K-1}\end{pmatrix},\\ H_{conv}&=\begin{pmatrix}\rho v\\ \rho uv\\ \rho v^2+p\\ (\rho e_t+p)v\\ \rho_1 Y_1 v\\ \vdots\\ \rho_{K-1}Y_{K-1}v\end{pmatrix} \quad H_{diff}=\begin{pmatrix}0\\ \tau_{yx}\\ \tau_{yy}\\ u\tau_{yx}+v\tau_{yy}-q_y\\ \rho_1 Y_1 V_{y,1}\\ \vdots\\ \rho_{K-1}Y_{K-1}V_{y,K-1}\end{pmatrix}. \end{aligned} \tag{4}$$

Here, ρ, u, v, e_t, ρ_i, $\dot{w}_i$, and Y_i are the total density, the velocity in the *x*-direction, the velocity in the *y*-direction, the total energy per unit mass, the density of the *i*th species, the mass production rate of the *i*th species and the mass fraction of the *i*th species, respectively.

The viscous stress tensors [39] are given as：

$$\tau_{xx}=\mu(\frac{4}{3}\frac{\partial u}{\partial x}-\frac{2}{3}\frac{\partial v}{\partial y}),\ \tau_{xy}=\tau_{yx}=\mu(\frac{\partial v}{\partial x}+\frac{\partial u}{\partial y}) \text{ and } \tau_{yy}=\mu(\frac{4}{3}\frac{\partial v}{\partial y}-\frac{2}{3}\frac{\partial u}{\partial x}). \tag{5}$$

The heat flux is assumed to obey Fourier's law and its dependence on interspecies diffusivities is fully considered：

$$q_x=-k\frac{\partial T}{\partial x}-\rho\sum_{i=1}^{K}h_i D_i\frac{\partial Y_i}{\partial x}, \tag{6}$$

$$q_y = -k\frac{\partial T}{\partial y} - \rho\sum_{i=1}^{K} h_i D_i \frac{\partial Y_i}{\partial y}. \tag{7}$$

The enthalpy of the gas mixture is denoted by h; h_i is the enthalpy of the ith species. The contribution of each species to the total energy is obtained by using a mass fraction averaged enthalpy, i.e.,

$$h = \sum_{i=1}^{K} Y_i h_i \,, \tag{8}$$

where
$$h = e_t + p/\rho - \frac{u^2 + v^2}{2}. \tag{9}$$

In order to close the system of equations, the ideal gas law for the average mixture properties is derived from the partial pressure equation for each species, that reads

$$p = \sum_{i=1}^{K} p_i = \sum_{i=1}^{K} \rho Y_i R_i T = \rho R T \quad \text{with} \quad R = \sum_{i=1}^{K} Y_i R_i,\ R_i = \frac{R}{W_i}, \tag{10}$$

where R is the universal gas constant and W_i the molar mass of each species.

The dynamic viscosity of the mixture is obtained using a modified Wilke mixing rule [40], and the Mathur mixing rule [41] is used for the thermal conductivity. The mass diffusion values are described by a multi-component diffusion model with thermal and pressure diffusion. A detailed hydrogen/air reaction model is adopted with 12 species and 42 elementary reactions [15].

2.2.3 Numerical scheme

The open-source framework AMROC is used for adaptive mesh refinement; dimensional splitting is employed in the numerical scheme. It is reported that, when considering the reactive source term utilizing the first-order accurate Godunov

splitting or the second-order accurate Strang splitting, the difference is usually small [9, 42]. Therefore, the computationally more efficient Godunov splitting method is employed for the decoupling of the chemically reactive source term in the present work. The second-order accurate MUSCL-TVD FVM (Finite Volume Method) is applied for discretization of the convective part of the NS equations. And the second-order accurate CD (Central Difference) scheme is used for the diffusion terms. As for the reactive source term, the fourth-order accurate semi-implicit GRK4A method is utilized for the integration, avoiding a globally coupled implicit problem. Additional restrictions are imposed on the time integration by the time-explicit CD scheme. It is relatively easy to use explicit multi-stage time integration methods for the implementation with SAMR. Because of the stability properties of the explicit integration schemes, the preferred practical methods with the ability of inexpensive time adaptation in SAMR are Runge–Kutta methods. Here, the optimal second-order SSP (Strong Stability Preserving) Runge–Kutta scheme is used with a CFL parameter 0.98 in combination with time splitting.

3 Experimental results

3.1 Experiment verification

Fig.2(a) shows the pressure recordings in the main pipelines. In order to precisely control the gaseous mass flux rates, orifice plates are installed in these pipelines. The orifice plates are calibrated using a standard sonic nozzle with a relatively error below 5% and are further modified based on the calibrated results. *Airmain*, *Nozzlemain*, O_2*main* and H_2*main* represent the upstream pressures of the air

in the air preheater, the hydrogen in the nozzle, the oxygen in the air preheater and the hydrogen in the air preheater. As shown in Fig.2(a), the pressures in the four pipelines remain relatively stable, and constant static pressures can be achieved quickly after a short pressure drop, when the valves are opened during the test period, indicating that a stable supply of the mass fluxes can be ensured.

Fig.2(b) shows the pressure variation in the air preheater. The initial pressure is zero. The valves of the air and oxygen in the air preheater are opened at t_1 and t_2, respectively. After the valve of the hydrogen and the spark plug in the air preheater are opened at the same time of t_3, the pressure in the air preheater undergoes a fast increase, and finally reaches a relatively stable state at t_4. This indicates that the air preheater is ready for stable operation at t_4, which is in agreement with the record of Fig.2(a). As shown in Fig.2(b), the total pressure for stable operation is Pbc=1.8 MPa, with the effective working time of t_5-t_4. During the operational interval the hydrogen is injected into the supersonic flow from the end of the Laval nozzle, and the uniform supersonic combustible mixture is produced after undergoing turbulent mixing with the supersonic air flow in the premixing duct. When the experiment is completed, the valve of the nitrogen in the air preheater is opened to replace the remaining combustible mixture in the whole apparatus at t_5.

The Mach number of the supersonic combustible mixture is 3.0; the molar ratio of the mixture $H_2/O_2/N_2$ is MR = 0.56:1.0:2.9, with the equivalence ratio (ER) 0.28. The flow velocity of the mixture is set to 1532 m/s, with the static pressure and temperature of 36.1 kPa and 581 K, respectively. Previous experimental investigations

[43] have demonstrated that when the static temperature does not exceed 800 K, the pre-ignition of the combustible mixture in the premixing duct can be effectively prevented when the equivalence ratio is below 0.45.

Fig.3(a) depicts the pressures at the three pressure sensors on the top wall of Win 2. The average static pressure of the supersonic combustible mixture is approximately 35 kPa, presenting an error of 1.1 kPa with the corresponding relative error of 3% compared with the theoretical value. As shown in Fig.3(a), when the spark plug in the hot jet tube ignites at t_4, the static pressure continues to increase gradually, indicating that the supersonic flow has not reached the stable state yet. The trigger of the spark plug introduces uncontrolled disturbances to the pressure sensors, which results in some uncertainty for the precise pressure measurement. Nevertheless, the relative error between the experimental measurements and theoretical calculation is reasonable, which also indirectly validates their accuracy.

The mass fluxes of the hydrogen and oxygen in the hot jet are 1.6 g/s and 16.4 g/s, respectively. In Fig.3(b), the maximal pressure in the hot jet tube reaches 0.67 MPa, which is 4.4 times of that before the ignition.

3.2 Propagating modes in experiments

Fig.4 visualizes the formation of a bow shock and its reflection on the upper wall. Note that throughout the experiment the supersonic flow of the reactive mixture is from right to left, as indicated by the arrow. In order to facilitate observation and analysis, the experimental images are all flipped vertically. After the injection of a hot jet into the supersonic flow, a bow shock is induced by the hot jet, as shown in

Fig.4(a). The high pressure behind the bow shock propagates upstream through the subsonic channel within the boundary layer on the lower wall, which further results in boundary layer separation in front of the bow shock due to the adverse pressure gradient and the subsequent generation of a recirculation zone, as shown in Fig.4(b). The mixing between the high-enthalpy product in the hot jet and the combustible mixture behind the bow shock enhances the consumption of the unburned reactant. The produced chemical heat release can further increase the pressure and temperature behind the bow shock, hence resulting in gradual lifting up of the bow shock [5-6]. In addition, a new shock bifurcation is observed along with the separated shock and the reflected shock, as the bow shock interacts with the boundary layer on the upper wall. As shown in Fig.4(c), the angle* of the bow shock is 5% larger than that in Fig.4(a), indicating the strength enhancement of the bow shock due to mixing and combustion behind the bow shock. The shock bifurcation further becomes larger, because the bow shock gradually becomes more pronounced and the adverse pressure gradient increases. As a result, it is found that the bifurcated shock structure occupies a larger part of the bow shock.

Knystautas et al. [44] carried out investigations for direct initiation of detonations using a hot jet of combustion products, indicating that the rapid turbulent mixing of the products in the hot jet with reactants is essentially the same as the combustion process in a propagating high-speed turbulent flame. It is reported that by

* The flow field of the detonation in the experiment is visualized using the High-speed Photron Fastcam SA-X2 camera, which can continuously provide the coordinates of the whole flow field subject to the set time interval. Based on the coordinates the shock angle we calculated the shock angle.

using a strong turbulent hot jet for ignition the flame-acceleration process of the transition from deflagration to detonation is entirely bypassed, thus prompting the rapid initiation [45]. However, rather than the direct jet initiation, due to the limited strength of the hot jet utilized the mechanism responsible for detonation initiation in the present work is actually a DDT with gradual flame acceleration. The interaction between the shock wave and the boundary layer is much more prominent during the whole jet induced DDT process. The formation of the shock bifurcation and the recirculation zone produce a region with low velocity, which can enhance the mixing between the burned product in the hot jet and the unburned reactant behind the bow shock inside this region, which further facilitates the consumption of the unburned gases together with the chemical heat release and eventually accelerates the DDT process.

3.2.1 Oblique shock-induced combustion/Mach stem-induced detonation (OSIC/MSID)

The combination of the turbulent combustion zones on the lower and upper walls promotes the formation of oblique shock-induced combustions in the vicinity of the channel walls and a Mach stem in the center flow, which propagates forward quickly towards the supersonic incoming flow.

As shown in Fig.5, the time interval of the three successive frames is $\Delta t = 50\ \mu s$, and therefore by further measuring the propagation intervals the relative and absolute propagation velocities are calculated as $\Delta V = 382\ m/s$ and $V_s = V + \Delta V = 1914\ m/s$, respectively. The theoretical CJ velocity under this

condition is $V_{CJ} = 1431$ m/s calculated with Cantera [46]. It is shown that the propagating velocity of the structure combined with the oblique shock-induced combustions and the Mach stem is 33% higher than the corresponding CJ velocity.

During the period of t_5-t_4 in Fig.3(a), there exists an obvious pressure increase with the ratio of $p/p_0 = 5.43$. The theoretical pressure rise ratios of CJ detonation and oblique shock wave are shown as follows [45]:

$$\frac{p}{p_0} = \frac{\gamma_0 Ma^2 + 1}{\gamma_1 + 1}, \tag{11}$$

$$\frac{p}{p_0} = \frac{2\gamma(Ma\sin\theta)^2}{\gamma+1} - \frac{\gamma-1}{\gamma+1}. \tag{12}$$

Here, $\gamma = \gamma_0 = \gamma_1 = 1.3$, $Ma = \frac{V_s}{V} \times 3 = 3.75$ and $\sin\theta = 0.41$. Therefore, the pressure rise ratios are 8.38 and 2.54 for CJ detonation and oblique shock wave, respectively. The measurement value is within this range, which can further confirm that the oblique shock waves on the lower and upper walls are either detonations or pure shock waves, but most probably oblique shock-induced combustion waves. The chemical heat release behind the oblique shocks increases the temperature and pressure behind; however, the reacted fronts are obviously separated with the oblique shocks. The Mach stem between the shock-induced combustion regions is located in the middle of flow, and approximately occupies 1/6 of the height of the whole channel, and a violent reaction zone can be observed behind it. The Mach stem induces a detonation wave with the overdrive degree of 1.77 ($f = [V_s/V_{CJ}]^2$), which is in fact a locally strongly overdriven detonation. Therefore, it can be concluded that the overall structure in Fig.5 is the oblique shock-induced combustions/Mach stem-induced

detonation (OSIC/MSID). As previously mentioned, the absolute propagating velocity of the OSIC/MSID is 1.33 times the CJ velocity, which also agrees with the previous work [47].

Fig.6 illustrates the schematic of the OSIC/MSID structure in detail. In the middle of the main stream is the Mach stem **MS** that is actually a detonation wave due to the tight coupling with the reaction front **RF** following behind. Directly behind the triple points are the slip lines, which are further developed into highly unstable shear layers **SS** because of the KH instability. The turbulent boundary layers **TBL** are generated on the walls and interact with the MSID, finally resulting in the formation of the recirculation zones **RCZ** and the separated oblique shocks **OS.** Behind the oblique shocks are the long and narrow reaction zones **RZ** decoupled with the oblique shocks, i.e., the OSIC. These structures together form the bifurcated detonations.

The recirculation zone is essentially of constant pressure and without the onset of combustion. Therefore, the highly unstable shear layer is induced within the interface between the shock-induced combustion zone and the unreacted area, and then converged with the transverse wave **TW**. The combustible mixture in the recirculation zone is consumed gradually through the subsequent turbulent mixing and diffusion effect. In addition, the flow field behind the MSID in the middle main stream is compressed due to the extrusion effect imposed by the high pressure product produced by the OSIC. As a result, the shear layers behind the triple points of the MSID undergo a transition process from contraction to expansion. Therefore, in the middle main stream behind the MSID, a hydrodynamic Laval nozzle is generated

between the two shear layers, provided that the shear layers act as free boundaries. In this nozzle, one might expect also a hydrodynamic throat, which could induce a choking of the flow behind the front of the MSID, and might further facilitate the overdriven propagation of the detonation wave.

3.2.2 Oblique shock-induced combustion (OSIC)

The molar ratio of the combustible mixture $H_2/O_2/N_2$ is changed to MR = 0.58:1.0:2.9 with the equivalence ratio, ER = 0.29, while the other conditions remain the same. Fig.7 describes the structure of the flow field after the hot jet ignition, which is overall an oblique shock-induced combustion (OSIC) with the thwartwise V shape. Different from the structure in Fig.5, however the local MSID has vanished entirely in the middle of the main stream. As discussed above, the MSID in Fig.5 is overdriven; however, an overdriven detonation will gradually attenuate to the CJ state without external fluctuations [37-38]. The velocity in the turbulent boundary layers generated on the walls is relatively low compared with that in the main flow. Therefore, the numerous vortices generated in the vicinity of the boundary layers can effectively enhance the mixing effect, which further accelerates the consumption of the unburned gases behind the oblique shock waves along with the chemical heat release due to the strong viscosity transport. As a result, the whole structure of the OSIC can propagate more quickly compared with the central detonation wave, especially when the ER increases. When the ER is increased by adding more hydrogen fuel to the combustible mixture, the OSIC can release more chemical heat, thus enhancing the strength of the oblique shock wave and increasing the oblique

shock degree slightly. Compared with Fig.5, the degree of the oblique shock wave in Fig.7 slightly increases by 3.4% because of larger deflection angle ($\sin\theta = 0.424$). The OSIC gradually converges from the walls of the channel to the middle of the main stream, thus swallowing the MSID and eventually resulting in the formation of the pure OSIC with the thwartwise V shape.

Fig.8 shows the schematic of the OSIC. In the central main stream there does not exist a local Mach stem, which illustrates the main qualitative difference to Fig.6. When the OSIC converges in the middle of the main stream, a contact discontinuity represented by a slip line is formed, and the burned products are generated, which can be inferred from the violent turbulent flame behind in Fig.7.

3.3 Discussion

In the experiments, four types of propagating detonation modes have been observed: Symmetric OSIC/MSID, unsymmetric OSIC/MSID, symmetric OSIC and unsymmetric OSIC. The symmetric and unsymmetric characteristics of propagating modes mainly depend on the strength of the hot jet, and especially the DDT process which is intrinsically unstable involving various flame instability mechanisms [45]. In order to eliminate this uncertainty and to be able to focus on the propagating modes, the overall propagation modes in supersonic combustible mixtures are classified as two kinds: OSIC/MSID and pure OSIC, as mentioned above. Both propagating modes are mainly influenced by the boundary layers in supersonic combustible mixtures, which differ significantly from the quiescent case.

A series of experimental tests were carried out and the results are summarized in

Fig.9. Three domains (A, B, C) are obtained for propagating modes marked by different colors and lines. Domain A represents the OSIC, Domain B shows the OSIC/MSID, and in the common Domain C the transition between the two propagating modes can occur. As shown in Fig.9, the OSIC is not likely to be generated when the ER is larger than 0.36, while when the ER is lower than 0.28 it is almost impossible to produce the propagating mode of the OSIC/MSID in the supersonic flow field. When the ER is between [0.28, 0.36], as shown in the Domain C, both the two propagating modes can coexist together; however, most of the cases undergo a transition from the OSIC/MSID to the pure OSIC, not the other way around, indicating that the OSIC is more robust in the cases adopted here.

Han [47] found that when the height of the channel is four times of that in the present work the propagating mode of the OSIC/MSID is likely to occur, c.f. Ref. [37]. Apparently, the propagation mode in the supersonic combustible mixture is highly dependent on the channel height. When the channel height is large, the scale of the boundary layer occupies only a small part of the whole channel, thus resulting in the relatively weak effect on the evolution of the main stream and the subsequent MSID in the middle of the channel. However, when the channel height is small, the boundary layer effect contributes significantly to the formation of the overall structure. The OSIC produced by the boundary layer is able to play an important role in the middle main stream, eventually resulting in the disappearance of the local MSID and the formation of the propagation mode with the thwartwise V shape.

4 Numerical results

4.1 Grid resolution

It is reported that [48] for the one-dimensional ZND solution of a self-sustaining hydrogen-oxygen detonation with detailed reaction, even a resolution of $4\ \mathrm{Pts}/\mathrm{l}_{ig}$ is not sufficient to capture the maximum of the intermediate product H_2O_2 correctly, and at least 5 to 6 $\mathrm{Pts}/\mathrm{l}_{ig}$ are typically required. Meanwhile, it is also noted that in triple points even finer resolutions are required. However, around multi-dimensional triple points, a higher resolution is expected to capture the internal wave structure completely. For regularly oscillating detonations, an effective resolution up to $44.8\ \mathrm{Pts}/\mathrm{l}_{ig}$ had been used in our previous two-dimensional verification simulations, which indicates that this resolution is sufficient for resolving secondary triple points [49].

However, in order to both accommodate the induction length reduction after the MSID gets overdriven when it propagates forward, and resolve the bifurcated detonation interaction with the boundary layer reliably, the computation here uses an effective highest resolution of $137.8\ \mathrm{Pts}/\mathrm{l}_{ig}$, which is achieved by a five-level refinement with refinement factors 2, 2, 2, 2, respectively. Specially, for efficiently resolving the boundary layer, a small region near the wall is refined compulsively to the highest level to ensure maximal grid resolution within the boundary layer.

4.2 Propagating modes in simulations

4.2.1 Oblique shock-induced combustion/Mach stem-induced detonation (OSIC/MSID)

Fig.10 shows the complexity of the oblique shock wave induced by the boundary layer on the walls and the Mach stem in the middle of the flow field for the $H_2/O_2/N_2$ mixture with the molar ratio 0.56:1.0:2.9. To distinguish between the simulated and the time in the experiment, the physical time in the following numerical simulations is denoted as $\tilde{t}$.

The overall structure shown in Fig.10(a) is qualitatively similar with that in Fig.5. It should be noted that besides the high temperature behind the Mach stem, as shown in Fig.10(b) the temperature near the wall is also very high due to the low velocity within the boundary layer. The highest temperature in the boundary layer even reaches approximately 2100 K, thus resulting in auto-ignition in the vicinity of the walls. As a result, it is observed that in Fig.10(b) the violent combustion also occurs behind the oblique shock waves along with the region in the central flow behind the Mach stem.

In order to achieve accurate numerical results, all physically relevant scales should be resolved, in spite of the order of accuracy of the numerical method. As for detonation simulations, there are multiple length scales, especially the diffusive scales for the viscous detonations solving the NS equations. It is reported that the diffusion effect including viscosity, heat and mass diffusion, mainly occurs in shear layers [17], and for hydrogen and hydrocarbon detonations typically the viscous shear thickness is

the smallest scale followed by the mass and then the heat diffusion thickness [21]. Therefore, the resolution of the smallest length scale, i.e., the viscous shear layer thickness ($\delta_{\text{visc}} = \sqrt{\mu t/\rho}$), is checked for the presented results. The viscosity is estimated using the average density (0.846 kg/m^3), temperature (1948 K) and pressure (4.888×10^5 Pa) at the top and bottom of the shear layer behind the lower triple point of the MSID in Fig.10. The viscosity for these average parameters is calculated as 6.619×10^{-5} Pa·s. Here the time at which the shear layer begins to become unstable is utilized for the viscous scale, which is obtained as $\delta_{\text{visc}} = 5.59\times10^{-5}$ m. The highest mesh resolution is smaller than the viscous scale, and about 5 cells are within the viscous scale, suggesting that these diffusive scales can be fully resolved.

Note that the smallest shock thickness found in the Mach stem for the MSID, is of the order of three or five mean free path lengths, which is not expected to be resolved. Further vortex stretching would genuinely not be represented in two space dimensions and thereby pseudo-DNS, rather than DNS, is performed in the present work.

Fig.11(a) illustrates the reaction zone using the OH mass fraction, which further confirms the occurrence of the chemical reaction both behind the Mach stem and near the walls. However, the reaction front near the wall behind the oblique shock wave is completely separated from the oblique shock front, indicating that only the OSIC is generated instead of the oblique detonation, which is also verified in Fig.10.

In the middle of the main stream, it is found in Fig.11(b) that the lower half of the reaction front is tightly coupled with the Mach stem, indicating the formation of a

locally strong overdriven detonation. The upper half of the reaction front is approximately 1.0 mm away from the Mach stem, but the separation distance is still not more than half of the corresponding induction length (l_{ig} = 2.153 mm), indicating that the upper half can be regarded as a local detonation. Between the OSIC and MSID is a large unburned jet flow, which can be further consumed by mixing and diffusion effects [52-53]. Pressure wave interactions are generated because of fluctuations in the chemical heat release rate in the combustion zone near the wall, which further return to interact with the oblique shock waves, as shown in Fig.12. In Fig.12(a)-(c), it is found that some unburned pockets are created in the OSIC, which are marked with red circles. These unburned gases are gradually consumed through the mixing effect as indicated by the numerous vortices generated by hydrodynamic instabilities (e.g. the KH instability, RM instability), and the baroclinic vorticity generation mechanism [54-56] behind the oblique shock wave. Especially the small-scale unburned pocket generated in Fig.12(a) almost disappears entirely in Fig.12(b)(c). When the unburned pockets are reacted, some extra chemical heat is released which can result in additional fluctuations. Through the comparison between Fig.12(a) and (c), it is found that when the small-scale unburned pocket is first consumed, a large-scale vortex is generated due to the extra chemical heat release. This can further enhance diffusion and mixing effects, thus resulting in larger pressure wave fluctuations.

As a result, it is observed that the oblique shock is not entirely straight due to the pressure wave interactions produced by the fluctuations in the chemical heat release.

Besides unburned pockets in the OSIC, the highly unstable shear layers in Fig.12(d)-(f) can also produce pressure wave fluctuations, which further have a significant influence on the overall structure. Large-scale vortices are generated along with the highly unstable shear layers and can contribute more significantly to the mixing effect than that in Fig.12(a)-(c). The enhanced mixing accelerates consumption of the unburned gases behind the oblique shock wave more efficiently, eventually resulting in larger fluctuations of the oblique shock wave. Due to the unstable combustion induced by the boundary layers, it is found that the OSIC on the top and bottom walls are not completely symmetrical, eventually resulting in the unsymmetrical MSID. This phenomenon of unsymmetric OSIC/MSID in the simulation is in agreement with the experimental observations as previously discussed in Section 3.3. It is believed that the unsymmetric structure of the OSIC/MSID mode can play an influential role in the structure stability of the engine combustor, which requires further study.

Fig.13 shows pressure oscillations from five straight lines parallel to the X axis between [3.5, 8.0] cm which are at Y=4.15cm, 4.16cm, 4.17cm, 4.18cm, and 4.19cm, respectively. The pressure records in the boundary layer near the wall present high fluctuations due to the turbulent combustion in the boundary layer. It is found that the pressure directly behind the oblique shock wave almost reaches a maximal value of 175 kPa together with a descending trend. This is quantitatively in agreement with the approximate average 170 kPa in Fig.3(a) when the overall structure of OSIC/MSID propagates forward.

It should be noted that the Mach stem in the middle of the main stream is slightly

oscillating due to the fluctuations of the oblique shock waves resulting from the unstable combustion on the walls, as shown in Fig.14. Nonetheless, the reaction front is still tightly coupled with the Mach stem, continuously maintaining a dynamically unstable MSID in the central flow.

4.2.2 Oblique shock-induced combustion (OSIC)

Fig.15 shows numerically the oblique shock wave associated with the combustion induced by the boundary layers on the walls for the $H_2/O_2/N_2$ mixture with the molar ratio 0.58:1.0:2.9, while the other conditions are all kept the same with that in Section 4.2.1.

The overall structure shown in Fig.15(a) is qualitatively similar with that in Fig.7. As shown in Fig.15(b), the temperature near the wall reaches approximately 2400 K. This temperature is 14% higher than that in Fig.10, which is high enough to induce the auto-ignition in the vicinity of the walls. Different from Fig.10, no Mach stem is generated in the central flow to induce the MSID, but only oblique shock wave reflections are formed. Fig.15(b) also illustrates the reaction zone, which further confirms the occurrence of the chemical reaction both behind the oblique shock waves and near the walls. The reaction fronts behind the oblique shock waves are completely separated from the oblique shock fronts, indicating that only the OSIC is generated instead of the oblique detonation.

Due to the higher chemical reactivity of the mixture with a larger ER compared with that in Section 4.2.1, the unstable combustion on the walls behind the oblique shock waves introduce relatively more instabilities, hence resulting in larger

fluctuations of the oblique shock waves and even formation of shock bifurcations, as shown in Fig.16. Nonetheless, a dynamically unstable OSIC is continuously maintained.

4.3 Discussion

4.3.1 Adiabatic wall boundary condition

From the experimental and numerical comparisons between Section 3.2 and Section 4.2, it is found that the overall structures are very similar, including the OSIC near the wall and MSID in the middle of the main stream. However, the main difference occurs near the walls behind the oblique shock waves. In Figs.10 and 15 the reactants near the wall are almost fully combusted. While, in Figs.5 and 7 the reactants near the wall (sketched as the recirculation zones **RCZ** in Figs.6 and 8) are still unburned. Since the adiabatic, no-slip boundary condition is imposed at the wall, the temperature in the boundary layer is getting close to the high total temperature due to the low velocity in the boundary layer. This results in the auto-ignition of the combustible mixture in the vicinity of the wall behind the oblique shock wave. Gamezo et al. [29] and Oran and Gamezo [30] investigated numerically the shock wave interaction with the boundary layer formed by an incident shock in a shock tube. They observed a similar phenomenon of complete combustion near the wall, due to the utilization of an adiabatic no-slip wall boundary condition.

It is reported in Ref. [31] that the isothermal boundary condition should be physically more justifiable for the temperature in boundary layers. But in experiments when the detonation front passes by the wall temperature of the test section, it

becomes considerably hot even if water cooling is utilized. The increase of the wall temperature contributes significantly to the consumption of unburned gases behind the detonation front. Therefore, more accurate simulations will require consideration of a heat transfer model in the wall boundary conditions in order to both prevent the generation of an unrealistically high temperature in the boundary layer and properly increase the wall temperature after passage of the detonation front.

4.3.2 Three-dimensional effect

In the present work two-dimensional pesudo-DNS are carried out; however, the real turbulent flows are truly three-dimensional. The relation between the two-dimensional simulations and the three-dimensional nature of turbulent detonations is currently still very open. Turbulence in detonations is mostly generated by the RM instability through the baroclinic vorticity generation mechanism [57-58], which can lead to vorticity generation comparable to the system scale to a great extent. Another source of turbulence on small scales is the KH instability, which is commonly known to be less significant than the RM instability [30]. Noted that, for the certain flows under consideration, it is reported that rather than the commonly known the RM instability, large-scale vortices involved in highly unstable shear layers dominate the formation of the turbulent flow and the rapid turbulent mixing between unburned and burned mixtures [33]. Radulescu et al. [54, 59] suggested the mechanism as a source of turbulence behind the detonation front, which is also observed in numerical and experimental DDT studies [60-62]. Oran and Gamezo [30] carried out investigations of flame acceleration and DDT, and showed that

two-dimensional computations agree well with three-dimensional results and experimental observations. Even though the accelerating flame became more wrinkled in three-dimensional simulations, the overall flame development is dominated by the RM instability [22], concluding that the two-dimensional and three-dimensional simulations showed very similar results. Both theoretical analysis and high-resolution numerical simulations were utilized by Li and Zhang [63] to compare two-dimensional and three-dimensional growth rates of the RM instability. It was found that the three-dimensional growth rate in the nonlinear regime is about 20% larger and 25% faster than that in two-dimensional simulations. However, in the linear regime the growth rates of the instability were the same in two and three dimensions.

In the present study, the RM instability tends to be the dominant mechanism generating turbulent structures behind the detonation front. This is why the present two-dimensional computations are in good agreement with those in the experiments. However, to clarify the exact propagating modes of detonation wave in supersonic combustible mixtures due to detonation wave/boundary layer interaction, three-dimensional computations would be needed in the further study.

5 Conclusions

In the present work, experimental observations and numerical simulations are combined together to investigate initiation and especially propagation modes of detonations in supersonic combustible mixtures. The main findings of the present work are as follows:

1. A hot jet induced Deflagration to Detonation Transition (DDT) rather than a

direct jet initiation is generated in supersonic combustible mixtures due to the limited strength of the hot jet utilized. Because of limited channel width, the resulting detonation exhibits shock wave bifurcation generated due to the bow shock interaction with the boundary layer of the unreacted inflow. The region with low velocity in the recirculation zone resulting from the shock bifurcation contributes to the mixing between burned gases in the hot jet and precompressed unburned mixtures crossing through the bow shock, which can further facilitate the consumption of the unburned gases together with the chemical heat release and eventually accelerate the detonation wave propagation.

2. Two main propagating modes are observed after the hot jet ignition: OSIC/MSID and pure OSIC, which are highly influenced by the boundary layer. For the OSIC/MSID mode, in the middle of the main stream is a Mach stem induced overdriven detonation. For the pure OSIC mode, no Mach stem but an OSIC with the thwartwise V shape is generated due to the strength enhancement of the oblique shock waves resulting from extra chemical heat release.
3. The OSIC/MSID and pure OSIC modes are independent of the details of detonation ignition and primarily dependent on the detailed mixture and inflow conditions. Hence, they are easily reproduced and verified through quasi-steady pseudo-DNS detonation simulations. It is found that the OSIC/MSID is not completely symmetrical due to the unstable combustion

induced by the boundary layers, which agrees with experimental observations. For the pure OSIC mode, due to relatively more instabilities resulting from extra chemical heat release, larger fluctuations are observed along the oblique shock waves.

4. The current investigations underscore the importance of boundary layer interaction effects for detonation studies in narrow channels. For the configurations considered here, viscosity cannot be neglected. In order to increase prediction accuracy further, boundary conditions with realistic heat loss should be developed.

Acknowledgements

This work is supported by the National Natural Science Foundation of China (No. 11702323) and the National Foundation of Defense Technology (No. 3101032).

References

[1] S.N.B. Murthy, E.T. Curran, Prog. Astronaut Aeronaut. 137 (1991) 124-158.

[2] N.N. Smirnov, V.F. Nikitin, Int. J. Hydrogen Energy 39 (2014) 1122-1136.

[3] N.N. Smirnov, V.B. Betelin, R.M. Shagaliev, V.F. Nikitin, I.M. Belyakov, Y.N. Deryuguin, S.V. Aksenov, D.A. Korchazhkin, Int. J. Hydrogen Energy 39 (2014) 10748-10756.

[4] N.N. Smirnov, V.F. Nikitin, L.I. Stamov, D.I. Altoukhov, Int. J. Hydrogen Energy 40 (2015) 11059-11074.

[5] X.D. Cai, J.H. Liang, R. Deiterding, Z.Y. Lin, AIAA J. 54 (8) (2016) 2449-2462.

[6] X.D. Cai, J.H. Liang, Z.Y. Lin, R. Deiterding, F.C. Zhuang, Combust. Sci. Technol. 187 (4) (2015), 525-536.

[7] X.D. Cai, J.H. Liang, R. Deiterding, Z.Y. Lin , Int. J. Hydrogen Energy 41 (2016), 6917-6928.

[8] X.D. Cai, J.H. Liang, Z.Y. Lin, R. Deiterding, Y. Liu, Aerosp. Sci. Technol. 39 (2014) 442-455.

[9] R. Deiterding, Parallel Adaptive Simulation of Multi-Dimensional Detonation Structures, Ph.D. Thesis, Brandenburgische Technische Universität Cottbus, Cottbus, 2003.

[10] R. Deiterding, Comput. Struct. 87 (2009) 769-783.

[11] R. Deiterding, J. Combust. 2011(2011) 1-18.

[12] M. Berger, Adaptive Mesh Refinement for Hyperbolic Differential Equations Ph.D. thesis, Stanford University Stanford, California, 1982.

[13] M. Berger, J. Oliger, J. Comput. Phys. 53(3) (1984) 484-512.

[14] Z. Liang, S. Browne, R. Deiterding, J.E. Shepherd, Proc. Combust. Inst. 31(2) (2007) 2445-2453.

[15] C.K. Westbrook, Combust. Flame 46(1982) 191-210.

[16] E.S. Oran, J.W. Weber, E.I. Stefaniw, M.H. Lefebvre, J.D. Anderson, Combust. Flame 113 (1998), 147-163.

[17] K. Mazaheri, Y. Mahmoudi, M.I. Radulescu, Combust. Flame 113 (2012) 2138-2154.

[18] Y. Mahmoudi, N. Karimi, R. Deiterding, S.Emami, J. Propul. Power 30(2) (2014)

384-396.

[19] S. Paolucci, Z.J. Zikoski, D. Wirasaet, J. Comput. Phys. 272 (2014) 814-841.

[20] S. Paolucci, Z.J. Zikoski, T.Grenga, J. Comput. Phys. 272 (2014)842-864.

[21] J.L. Ziegler, R. Deiterding, J.E. Shepherd, D.I. Pullin, J. Comput. Phys. 230(20) (2011) 7598-7630.

[22] V.N. Gamezo, T. Ogawa, E.S. Oran, Proc. Combust. Inst. 31 (2007) 2463-2471.

[23] V.N. Gamezo, T. Ogawa, E.S. Oran, Combust. Flame 155 (2008) 302-315.

[24] D.A. Kessler, V.N. Gamezo, E.S. Oran, Combust. Flame 157 (2010) 2063-2077.

[25] G.B. Goodwin, R.W. Houim, E.S. Oran, Proc. Combust. Inst. 36 (2017) 2717-2724.

[26] G.B. Goodwin, R.W. Houim, E.S. Oran, Combust. Flame 173 (2016) 16-26.

[27] X.D. Cai, R. Deiterding, J.H. Liang, M.B. Sun, Y. Mahmoudi, J. Fluid Mech. (2017) in Press.

[28] Y.S. Weber, E.S. Oran, J.P. Boris, J.D.Jr. Anderson, Phys. Fluids 7 (1995) 2475-2488

[29] V.N. Gamezo, A.M. Khokhlov, E.S. Oran, Combust. Flame 126 (2001) 1810-1826

[30] E.S. Oran, V.N. Gamezo, Combust. Flame 148 (2007) 4-47.

[31] K.P. Grogan, M. Ihme, Proc. Combust. Inst. 35 (2015) 2181-2189.

[32] K.P. Grogan, M. Ihme, Proc. Combust. Inst. 36 (2017) 2927-2935.

[33] X.D. Cai, R. Deiterding, J.H. Liang, Y. Mahmoudi, Proc. Combust. Inst. 36 (2017) 2725–2733.

[34] J.H. Liang, X.D. Cai, Z.Y. Lin, R. Deiterding, Acta Astronaut. 105 (1) (2014) 265-277.

[35] X. Han, J. Zhou, Z.Y. Lin, Chin. Phys. B. 21 (2012) 124702.

[36] X. Han, J. Zhou, Z.Y. Lin, Y. Liu, Chin. Phys. Letters 30(2013) 054701.

[37] X.D. Cai, J.H. Liang, Z.Y. Lin, R. Deiterding, H. Qin, X. Han, ASCE J. Aerosp. Eng. 28 (1) (2015) 04014046.

[38] X.D. Cai, J.H. Liang, R. Deiterding, Combust. Sci. Technol. 188 (10) (2016), 1674-1690.

[39] F.A. Williams, Combustion Theory, The Benjamin/Cummings Publishing Company Inc., Menlo Park, California, 1985.

[40] R.B. Bird, W.E. Stewart, E.N. Lightfoot, Transport Phenomenon, 2nd ed., John Wiley & Sons, 2002.

[41] S. Mathur, P.K. Tondon, S.C. Saxena, Mol. Phys. 12(6) (1967) 569-579.

[42] Y. Mahmoudi, and K. Mazaheri, Operator Splitting in Simulation of Detonation Structure, Proceedings of the 22nd International Colloquium on the Dynamics of Explosions and Reactive Systems (ICDERS), Minsk, Belarus, 2009.

[43] Z.Y. Lin, Research on Detonation Initiation and Development Mechanisms in Elevated Temperature Supersonic Premixed Mixture, Ph.D. Thesis, National University of Defense Technology, Changsha, Hunan, 2008. (In Chinese)

[44] R. Knystautas, J.H.S. Lee, I.O. Moen, H.G. Wagner, Proc. Combust. Inst. 17 (1979) 1235-1245.

[45] J.H.S. Lee, The Detonation Phenomenon. New York: Cambridge University

Press, 2008.

[46] D. Goodwin, Tech. Rep. California Institute of Technology, http://www.cantera.org.

[47] X. Han, Research on Detonation Initiation and Propagation Mechanisms in Supersonic Premixed Flows, Ph.D. thesis, National University of Defense Technology, Changsha, Hunan, 2013. (In Chinese)

[48] R. Deiterding, G. Bader, Analysis and Numerics for Conservation Laws 2005 69-91.

[49] W. Crutcheld, M.L. Welcome, J. Sci. Program 2 (1993) 145-156.

[50] X.Y. Hu, B.C. Khoo, D.L. Zhang, Z.L. Jiang, Combust. Theory Model. 8 (2004) 339-359.

[51] X.Y. Hu, D.L. Zhang, B.C. Khoo, Z.L. Jiang, Shock Waves 14 (2005) 37-44.

[52] K. Mazaheri, Y. Mahmoudi, M. Sabzpooshani, M.I. Radulescu, Combust. Flame 162 (2015) 2638-2659.

[53] Y. Mahmoudi, K. Mazaheri, Acta Astronaut. 115 (2015) 40-51.

[54] M.I. Radulescu, G.J. Sharpe, J.H.S. Lee, C.B. Kiyanda, A.J. Higgins, R.K. Hanson, Proc. Combust. Inst. 30 (2) (2005), 1859-1867.

[55] Y. Mahmoudi, K. Mazaheri, Proc. Combust. Inst. 33 (2) (2010), 2187-2194.

[56] G.J. Sharpe, J. Fluid Mech. 447 (2001) 31-51.

[57] M. Brouillette, Annu. Rev. Fluid Mech. 34 (2002), 445-468.

[58] M. Lombardini, R. Deiterding, and D. I. Pullin, Quality and Reliability of Large-Eddy Simulations, Proceedings of QLES 2007 International Symposium,

Springer, The Netherlands, 2008, 283-294.

[59] M. I. Radulescu, G. J. Sharpe, C. K. Law, and J. H. S. Lee, J. Fluid Mech. 580 (2007), 31-81.

[60] A. M. Khokhlov, E. S. Oran, and G. O. Thomas, Combust. Flame, 117 (1999), 323-339.

[61] A. M. Khokhlov, E. S. Oran, A. Y. Chtchelkanova, and J. C. Wheeler, Combust. Flame, 117 (1999) 99-116.

[62] G. O. Thomas, R. Bambrey, and C. Brown, Combust. Theory Model. 5 (2001) 573-594.

[63] X. L. Li, and Q. Zhang, Phys. Fluids, 9 (1997) 3069-3077.

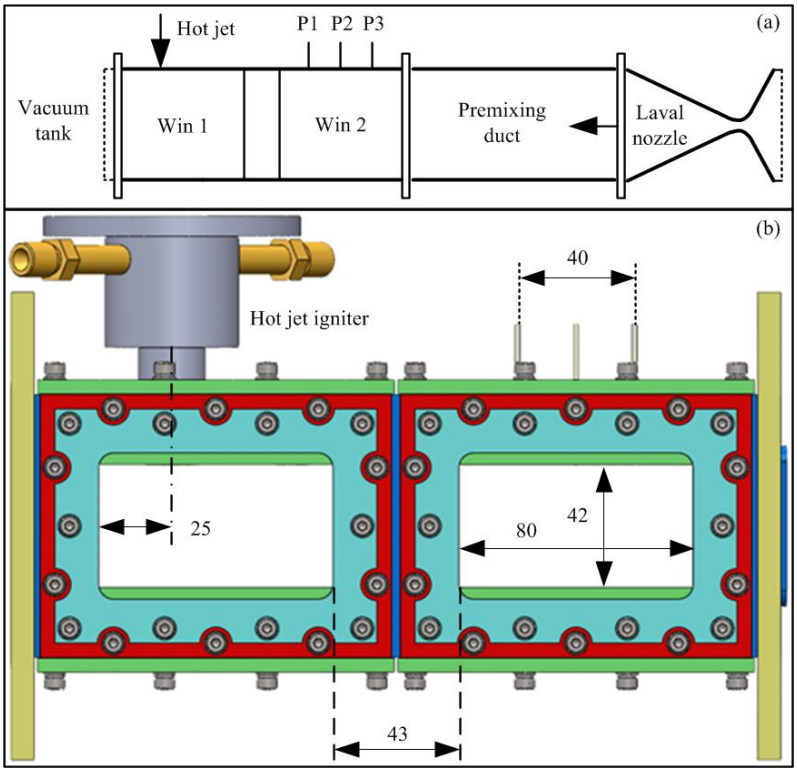

Fig.1 Schematic of the experiment setup, (a) experiment system and (b) test section; dimensions are in mm.

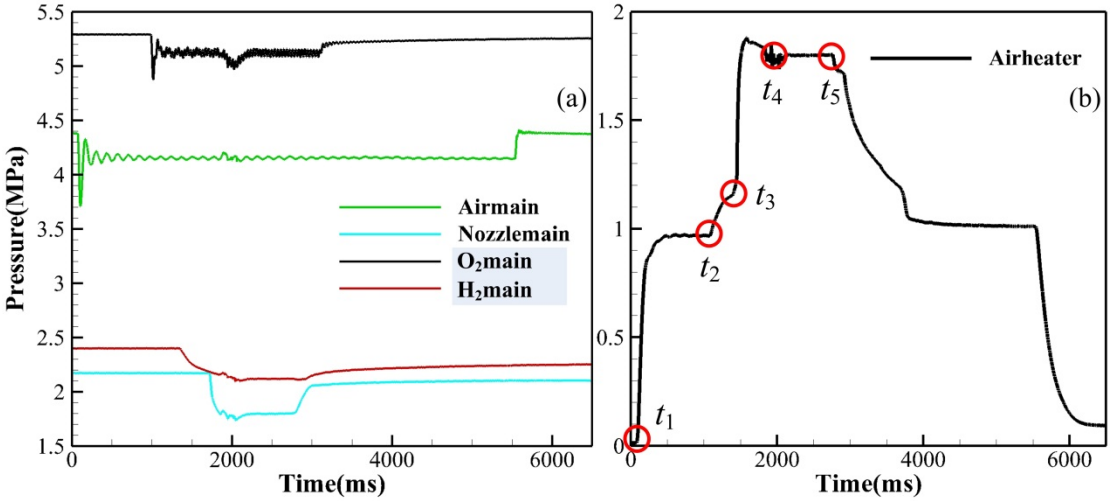

Fig.2 The pressure measurements in the main pipelines and the air preheater, (a) Pressures in the main pipelines, (b) Pressure in the air preheater.

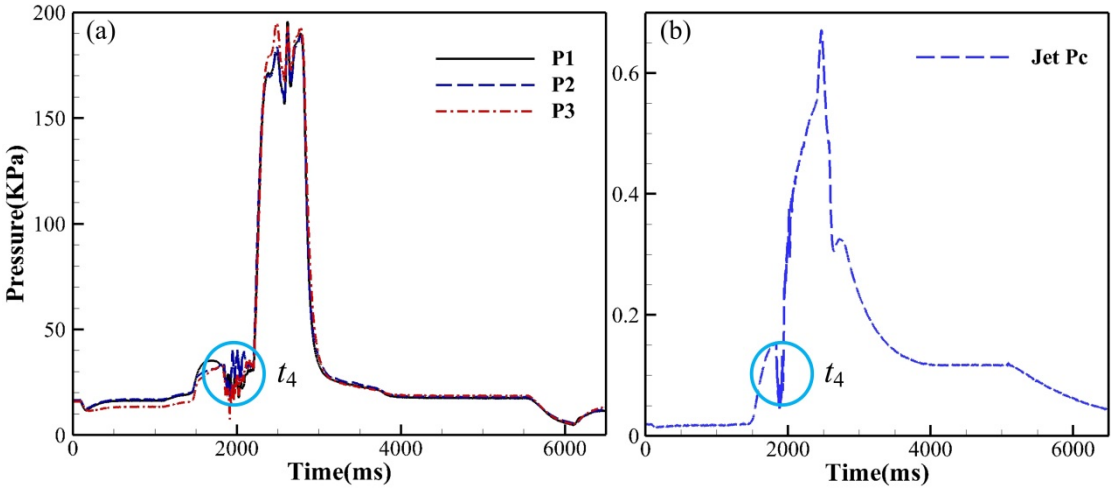

Fig.3 Experimental pressure measurement, (a) pressures in the premixing duct, (b) pressure in the hot jet tube.

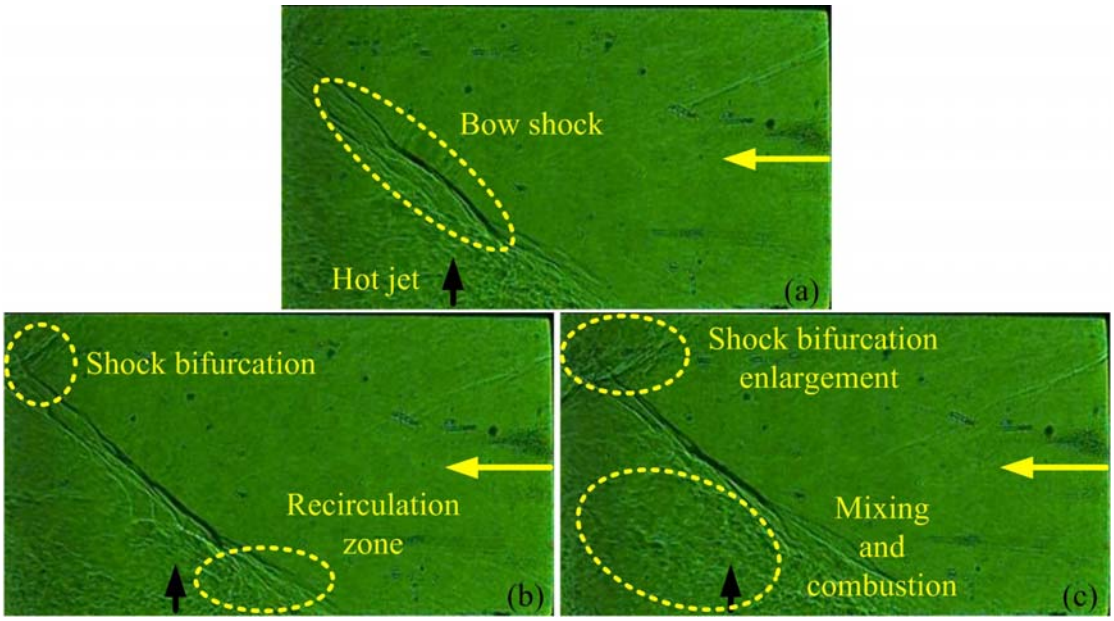

Fig.4 High-speed laser schlieren images showing the formation of the shock bifurcation after the injection of the hot jet into the supersonic combustible mixture, (a) $t = 778.08$ ms , (b) $t = 778.72$ ms and (c) $t = 779.36$ ms

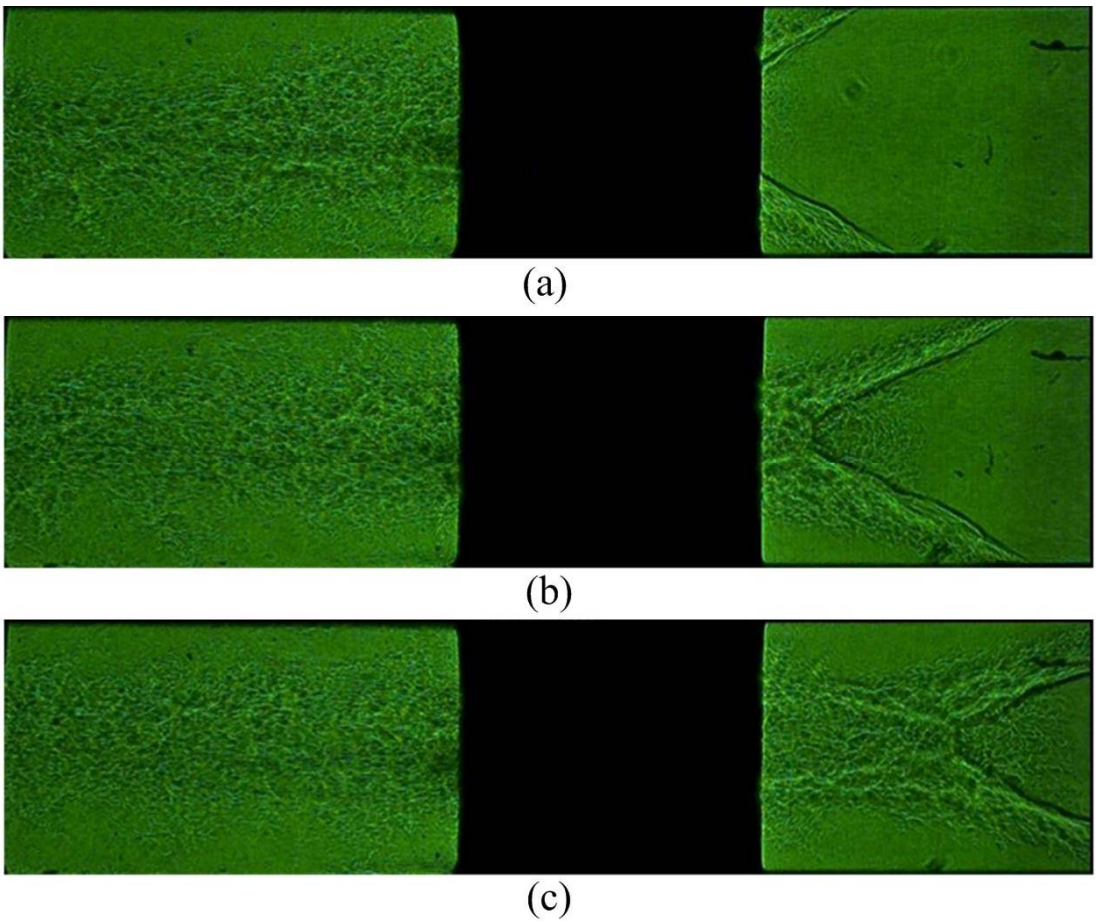

Fig.5 High-speed laser schlieren images for the OSIC/MSID, (a) $t = 958.45$ ms, (b) $t = 958.5$ ms and (c) $t = 958.55$ ms.

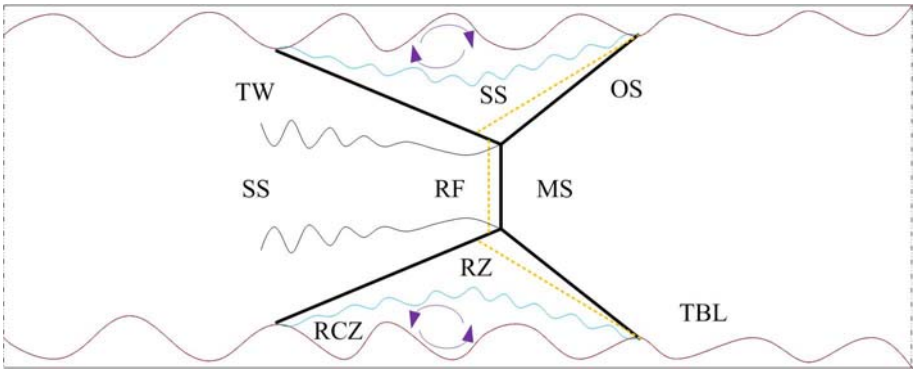

Fig.6 Schematic sketch of the OSIC/MSID configuration.

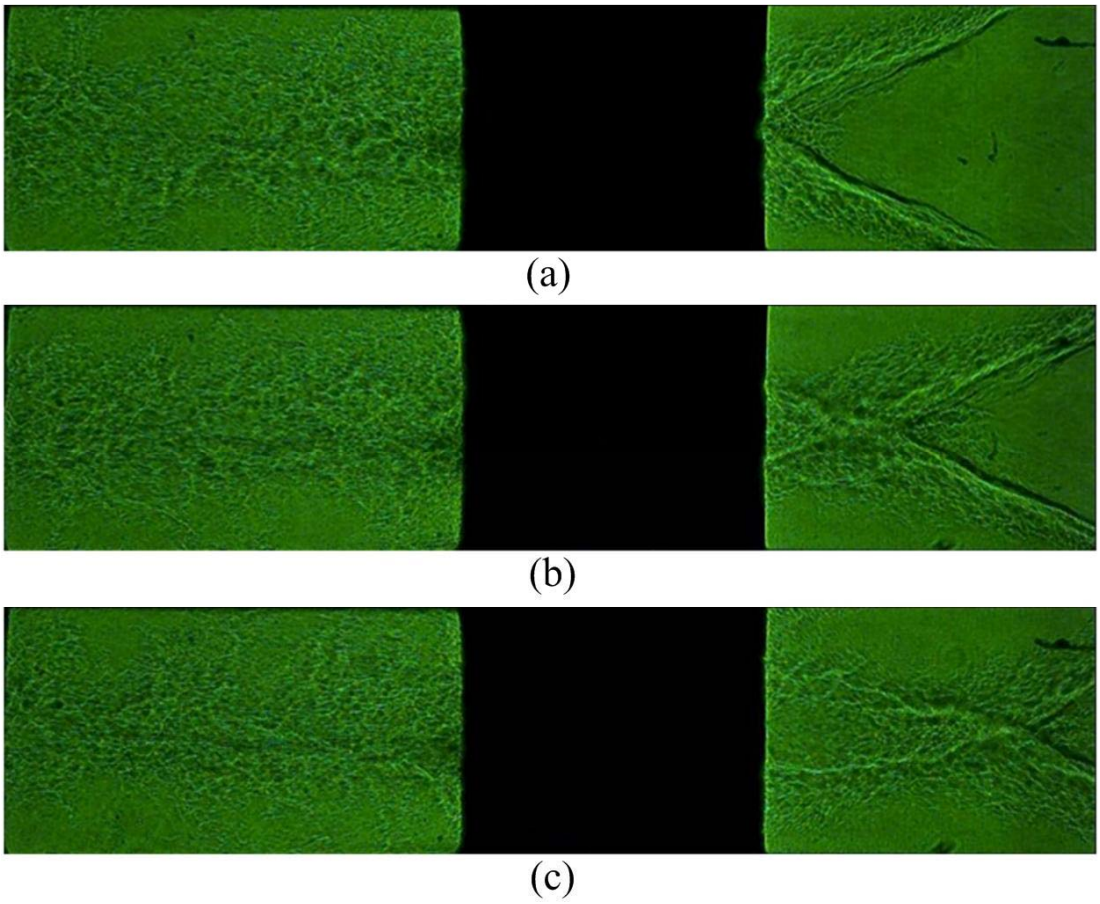

Fig.7 High-speed laser schlieren images for the OSIC, (a) $t = 833.95$ ms (b) $t = 834.0$ ms and (c) $t = 834.05$ ms.

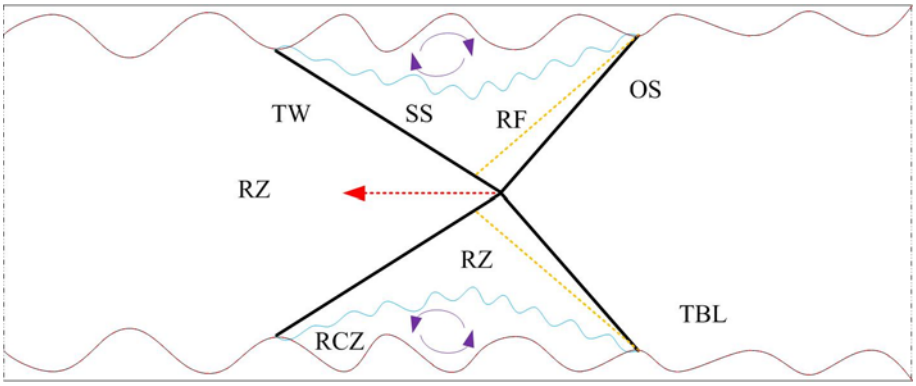

Fig.8 Schematic sketch of the OSIC.

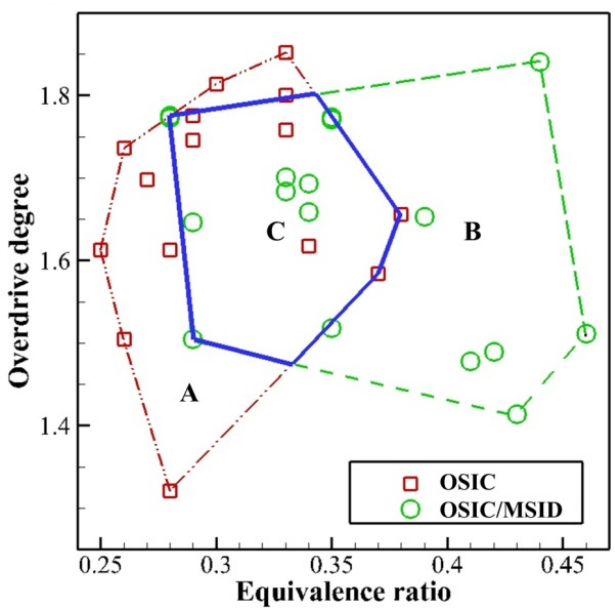

Fig.9 Distribution of the two propagating modes for the OSIC and OSIC/MSID.

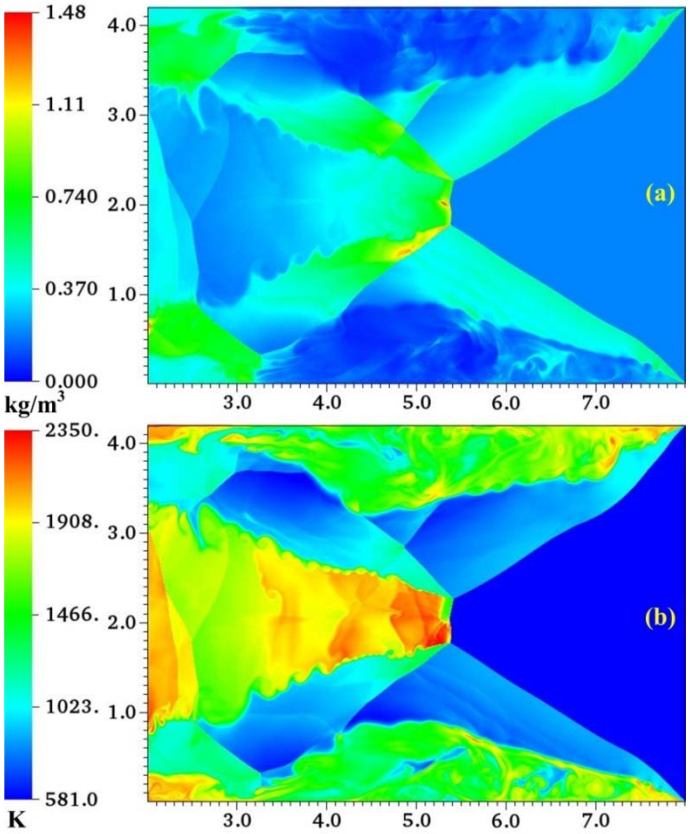

Fig.10 The OSIC/MSID structure at $\tilde{t} = 230\ \mu s$. Color plots of density (a) and temperature (b)

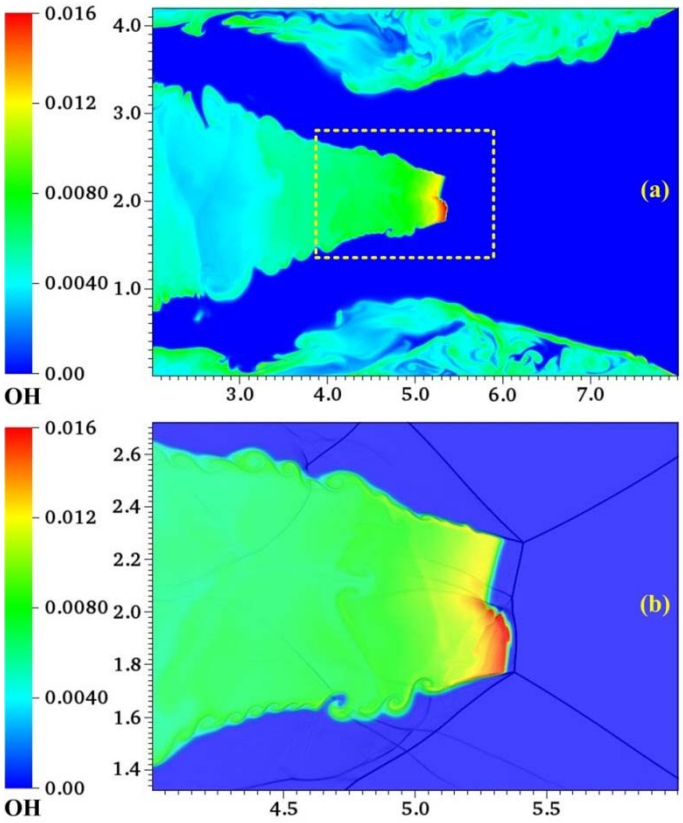

Fig.11 The reaction zones both near the wall and behind the Mach stem, (a) Color plot of OH mass fraction, (b) Enlargement of the MSID with shock fronts overlaid.

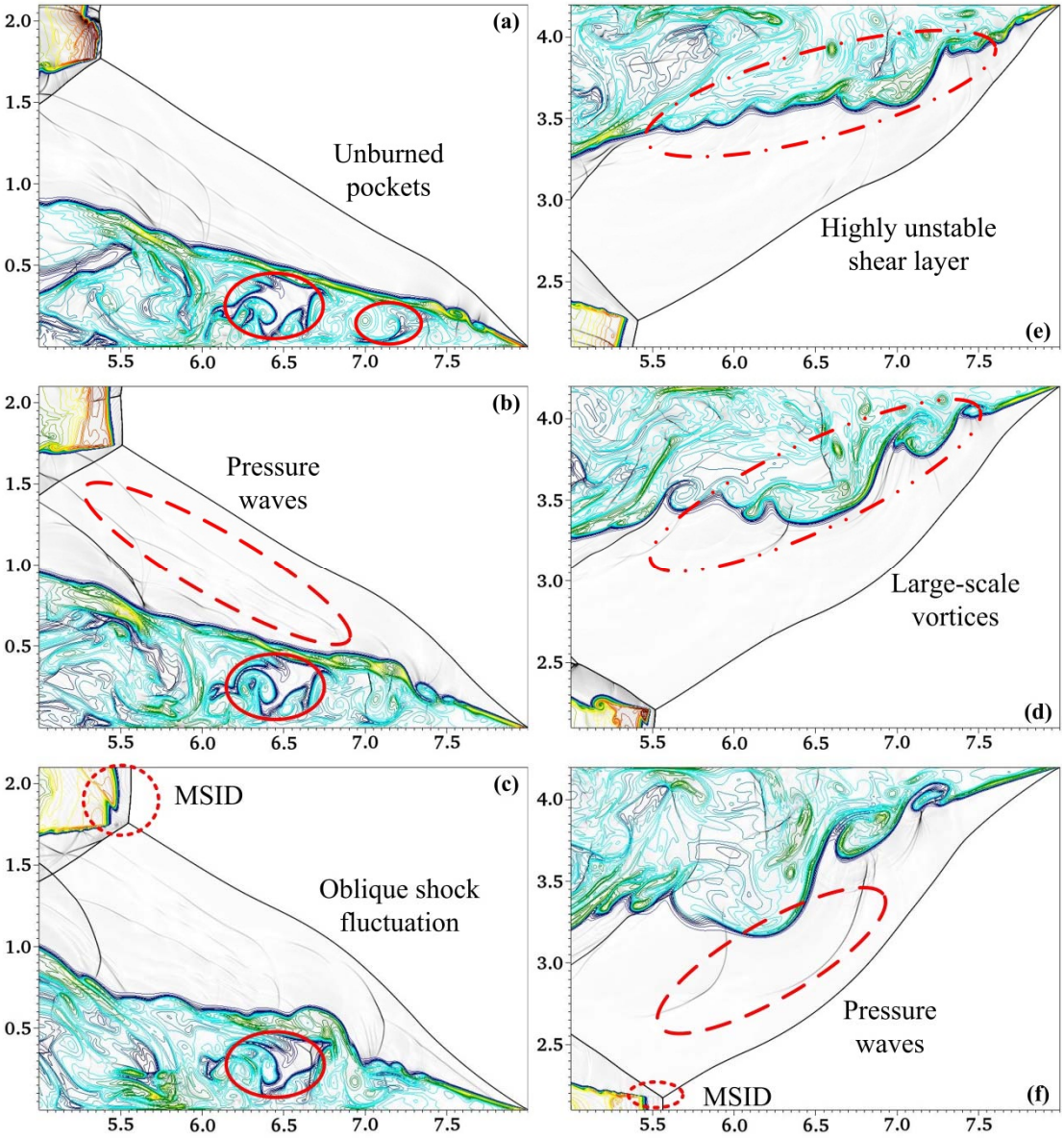

Fig.12 Isolines of OH mass fraction and numerical density schlierens illustrating detonation wave interactions with boundary layers both on the lower and upper halves, first row (a and e) $\tilde{t}$=230 μs , second row (b and d) $\tilde{t}$=235 μs and third row (c and f) $\tilde{t}$=240 μs .

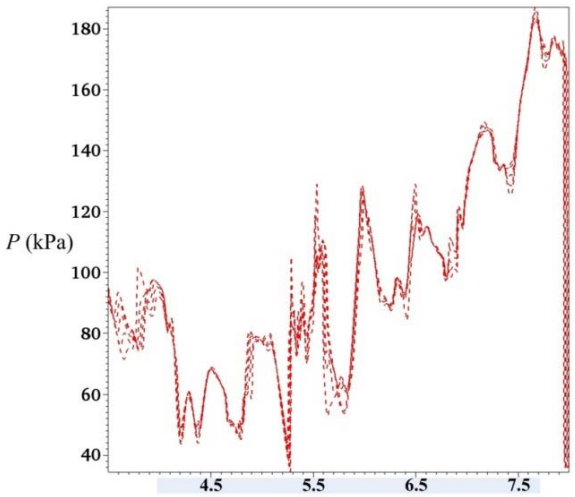

Fig.13 Pressure oscillations in the boundary layer near the wall.

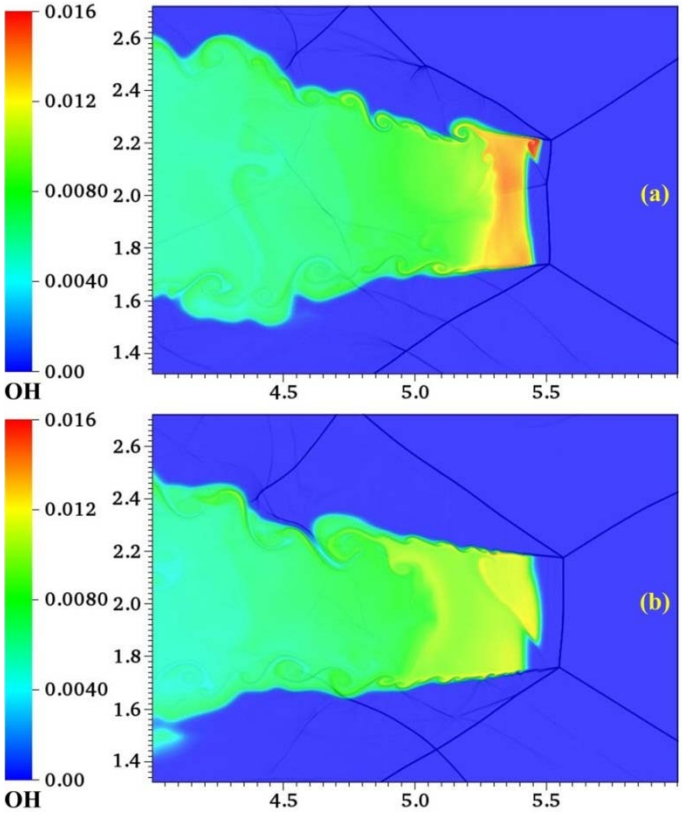

Fig.14 Enlargement of the MSID, color plot of OH with shock fronts overlaid, (a) $\tilde{t}$=235 μs, (b) $\tilde{t}$=240 μs.

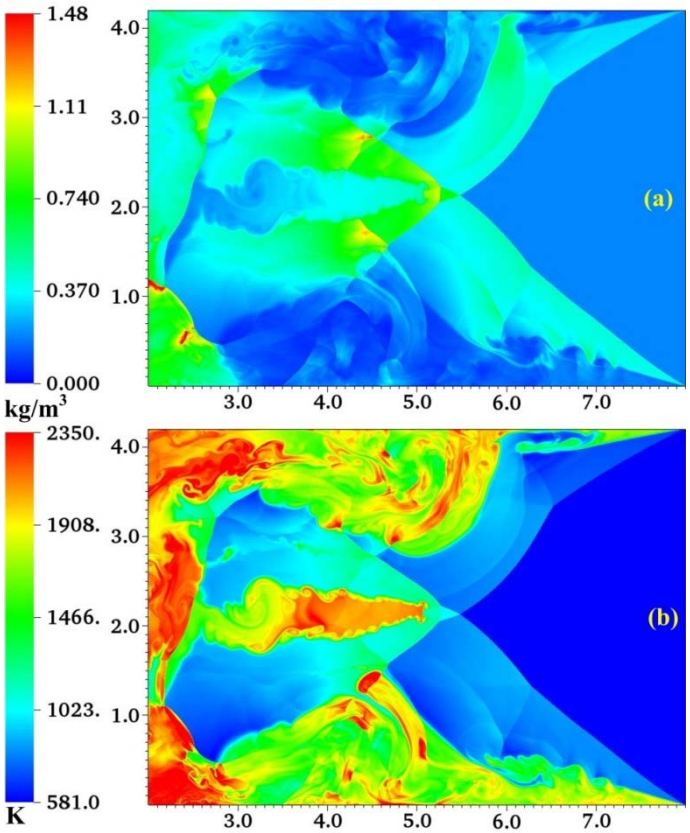

Fig.15 The OSIC structure at $\tilde{t} = 255\ \mu s$. Color plots of density (a) and temperature (b).

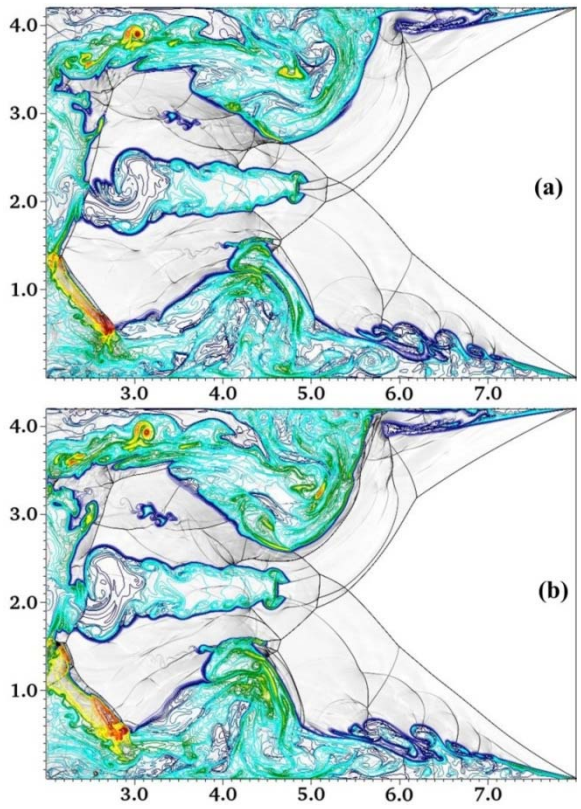

Fig.16 Isolines of OH mass fraction and numerical density schlierens for the OSIC,

(a) $\tilde{t}$=257.5 μs, (b) $\tilde{t}$=260 μs.